Parametrization of Extended Gaussian Disorder Models from Microscopic Charge Transport Simulations

Pascal Kordt,[*,†] Ole Stenzel,[‡] Björn Baumeier,[†] Volker Schmidt,[‡] and Denis Andrienko[*,†]

[†]Max Planck Institute for Polymer Research, Ackermannweg 10, 55128 Mainz, Germany

[‡]Institute of Stochastics, Ulm University, Helmholtzstraße 18, 89069 Ulm, Germany

S Supporting Information

ABSTRACT: Simulations of organic semiconducting devices using drift-diffusion equations are vital for the understanding of their functionality as well as for the optimization of their performance. Input parameters for these equations are usually determined from experiments and do not provide a direct link to the chemical structures and material morphology. Here we demonstrate how such a parametrization can be performed by using atomic-scale (microscopic) simulations. To do this, a stochastic network model, parametrized on atomistic simulations, is used to tabulate charge mobility in a wide density range. After accounting for finite-size effects at small charge densities, the data is fitted to the uncorrelated and correlated extended Gaussian disorder models. Surprisingly, the uncorrelated model reproduces the results of microscopic simulations better than the correlated one, compensating for spatial correlations present in a microscopic system by a large lattice constant. The proposed method retains the link to the material morphology and the underlying chemistry and can be used to formulate structure–property relationships or optimize devices prior to compound synthesis.
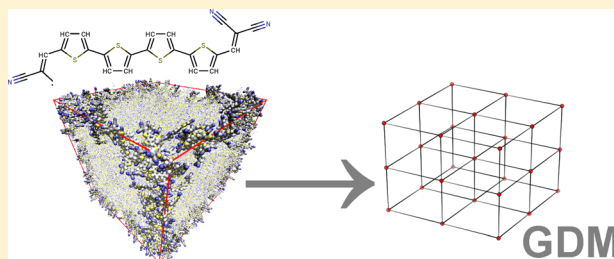
1. INTRODUCTION

The optimization of organic photovoltaic cells,[1,2] light emitting diodes,[3] and field effect transistors[4] requires the improvement of the charge-carrier mobility, μ, of an organic semiconductor, which depends on charge-carrier density, ρ, external electric field, $\mathbf{F}$, and temperature, T.[5–10] Different experimental setups have been proposed to measure these dependencies, e.g., time-of-flight,[11,12] field effect transistor,[13–15] diode,[3] microwave conductivity,[16] or charge extraction by linearly increasing voltage[17] measurements. They each operate at different charge densities and hence should be accompanied by an appropriate model in order to recover the full dependence.[18] Analytical expressions have therefore been proposed by analyzing various model systems[9,19–22] and are routinely used to interpret experiments[23–27] as well as to parametrize charge transport models. While being useful for the fine-tuning of the device performance for a specific material combination, these parametrizations do not directly relate the chemical structure or material morphology to charge mobility and hence cannot be applied to compound screening.

Computer simulations can help to retain the link to the chemical structure and should ideally provide the mobility μ as a function of ρ, T, and F over the ranges relevant for use in device simulations. At an atomistic level of detail, which is required for describing morphologies and charge transfer processes without fitting parameters,[28–31] it is possible to study only relatively small systems comprising up to several thousands of molecules and concomitantly at high carrier densities. Larger systems and thereby lower carrier densities can

be simulated by employing a stochastic model[32,33] parametrized on the distribution and correlation functions of atomistic simulations, both for morphologies and transport parameters. With the help of stochastic models, the dependence of mobility on charge density and field can, in principle, be tabulated and used to solve the macroscopic drift-diffusion equations. In practice, the range of charge densities accessible to stochastic simulations is still limited and pronounced finite-size effects occur,[34] especially at low densities. In this work we illustrate how to overcome these limitations and parametrize the analytical expressions resulting from the Gaussian disorder models. To do this, we tabulate the mobility as a function of charge density using microscopic (atomistic and stochastic) approaches, eliminate finite-size effects at small carrier densities, and then fit the data to the analytical forms provided by the extended and extended correlated Gaussian disorder models.

The approach is illustrated on an amorphous phase of dicyanovinyl-substituted quaterthiophene (DCV4T), whose chemical structure is shown in Figure 1a. DCV4T is a thermally stable dye[35,36] with a small optical band gap, which renders it as an excellent donor for bulk heterojunction solar cells.[37–42] When mixed with C60, DCV4T retains (at least partially) its crystallinity.[43–45] Here, however, we will study pure amorphous (glassy) systems, where morphological disorder results in a large energetic disorder and hence pronounced finite size
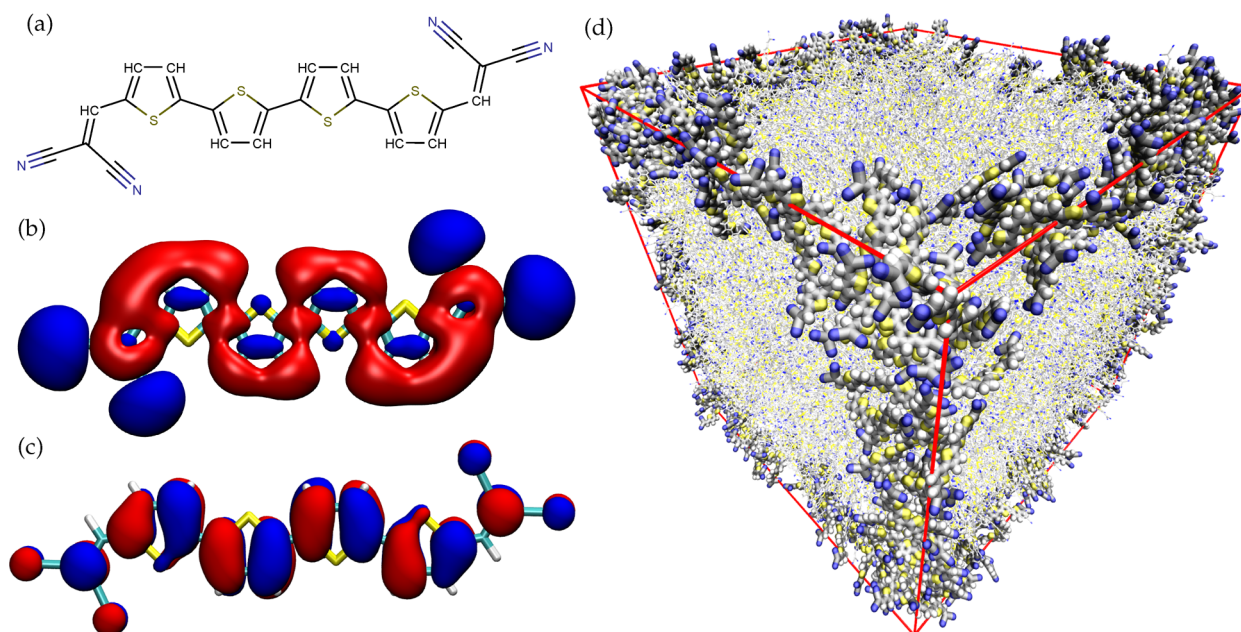
Figure 1. (a) Chemical structure, (b) electrostatic potential (at ±0.7 V), (c) highest occupied molecular orbital, and (d) amorphous morphology of 4096 molecules of dicyanovinyl-substituted quaterthiophene (DCV4T).

effects, making these systems ideal for illustrating and testing the method.

2. METHODOLOGY

To perform molecular dynamics simulations, the reparametrized[43,45] version of the OPLS[46,47] force field and the GROMACS package were used.[48] An amorphous phase of DCV4T has been generated using the isothermal–isobaric (*NPT*) ensemble with the Berendsen barostat and thermostat[49] by equilibrating 4096 molecules at T = 800 K for 10 ns, quenching the system to T = 300 K, and equilibrating again for 10 ns. The final cubic box of 13.7 nm × 13.7 nm × 13.7 nm is shown in Figure 1d.

Charge transport simulations were carried out using the VOTCA package.[28] The rates of a charge transfer reaction were evaluated using the high temperature limit of the Marcus theory[50,51]

$$\omega_{ij} = \frac{2\pi}{\hbar} \frac{J_{ij}^2}{\sqrt{4\pi\lambda_{ij}k_\mathrm{B}T}} \exp\left[-\frac{(\Delta E_{ij} - \lambda_{ij})^2}{4\lambda_{ij}k_\mathrm{B}T}\right] \quad (1)$$

where $\Delta E_{ij} = E_i - E_j$ is the energy difference between localized states, λ_{ij} is the reorganization energy, and J_{ij} is the electronic coupling. For each molecule i with center-of-mass coordinate $\mathbf{r}_i$ the site energy was calculated as $E_i = E_i^\mathrm{int} + E_i^\mathrm{el} + E_i^\mathrm{pol} + q\mathbf{F}\cdot\mathbf{r}_i$, where E_i^int is the internal molecular energy, i.e., the adiabatic ionization potential of the molecule. E_i^el is the electrostatic energy due to variations of the local electric field, evaluated using atomic partial charges. The corresponding electrostatic potential, which demonstrates the acceptor–donor–acceptor character of the molecule, is shown in Figure 1b. E_i^pol is the induction energy, evaluated using the Thole model,[52,53] $q\mathbf{F}\cdot\mathbf{r}_i$ is the energy due to the interaction of charged molecules with an external electric field. The corresponding parameters can be found in the Supporting Information of refs 43 and 45. Note that the acceptor–donor–acceptor architecture of DCV4T, in combination with nonplanar molecular geometries in the amorphous morphology, leads to large molecular dipole

moments and pronounced spatially correlated energetic disorder of σ = 0.253 eV.

Electronic couplings were evaluated for all molecule pairs in the neighbor list using the semiempirical ZINDO method.[54,55] The frozen core approximation was used, i.e., the HOMO orbital, which is shown in Figure 1c, provides the main contribution to the diabatic states of the dimer. The neighbor list was constructed using a cutoff of 0.7 nm between rigid fragments (thiophenes and dicyanovinyl groups).

The variable-step-size implementation of the kinetic Monte Carlo algorithm was used to solve the master equation[28] and simulate charge dynamics in the system. Coulomb interaction between charges was accounted for approximately by excluding double occupancy of a site. For 4096 molecules, 1–16 charges per simulation box were used, corresponding to hole densities of 0 (no interactions for a single charge carrier) to 6.22×10^{18} cm^{-3}, which covers typical values for OFET measurements.[18] Simulation times varied between 0.1 and 0.0001 s, depending on the number of carriers (systems with many carriers undergo faster relaxation). The mobility μ was evaluated by averaging over several trajectories and all carriers, $\mu = 1/NF^2 \sum_{k=1}^{N} \langle \mathbf{v}_k \cdot \mathbf{F} \rangle$, where $\mathbf{v}_k$ is the velocity of carrier k, and $\langle...\rangle$ denotes the average over the simulation time.

High computational costs limit the accessible system size in atomistic simulations. Therefore, a stochastic model[32,33] was used to reproduce distribution functions for center of mass positions, site energies, pair connection and transfer integrals. Positions were parametrized using the thinning of a Poisson process: we first generated a purely random pattern of points (candidates for site positions) such that the number M of points in a given volume V is Poisson distributed, $M \sim \mathrm{Poi}(\rho_\mathrm{site}V)$, with $\rho_\mathrm{site} > 1.59$ nm^{-3} denoting the density of points per unit volume. In a second step points that are too close to each other (i.e., the unphysical situation of overlapping molecules) were deleted by assigning a radius $R_n = r_h + X_n$ to each point and deleting those points for which a sphere of radius R_n is contained in the sphere of another point with radius $R_m > R_n$. Here $r_h = 0.1$ nm is the minimum separation observed
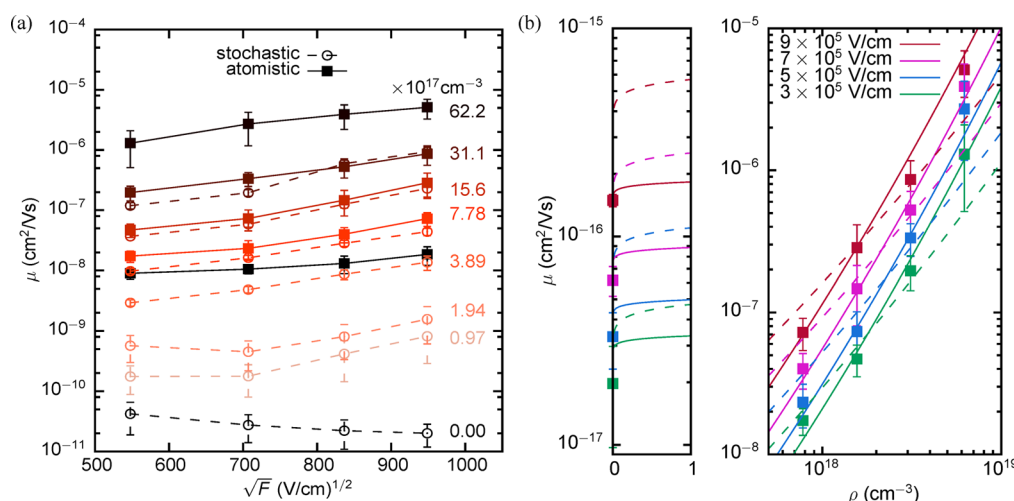
Figure 2. (a) Mobility versus the square root of applied field for charge densities ranging from 9.7×10^{16} (light color) to 6.2×10^{18} cm^{-3} (dark color). The zero-density limit is given in black. Solid lines correspond to the atomistic system (4096 molecules) while dashed lines represent a stochastic system (ca. 32 000 hopping sites). (b) Microscopic mobilities (squares) fitted to the EGDM (solid lines) and ECDM (dashed lines) models.

in the atomistic data and X_n is a (positive) Gamma-distributed random variable, mimicking the freedom in molecular orientation. The procedure was repeated until the desired density of $\rho_{site} = 1.59$ nm^{-3} was obtained, in agreement with the atomistic data. The stochastic model for site positions has been validated by comparing the atomistic and stochastic pair correlation functions $g(r)$ (see the Supporting Information for details).

Site energies with spatial correlation were generated using a moving-average procedure.[32,33] The main idea is to decompose the site energy into two contributions: one that is a site-specific Gaussian distributed random variable and another one that is the sum running over all neighbors, with another set of previously fixed Gaussian distributed random variables. Since any sum of independently Gaussian distributed variables is again Gaussian distributed, we obtain Gaussian distributed random variables with spatial correlation. The necessary parameters for the method are obtained by fitting the resulting correlation function $\kappa(r)$ against its atomistic counterpart (see Figure 3). The neighbor list of the stochastic model was generated by picking a point and connecting to it all neighboring points in a sphere of a radius $r_{min} = 0.633$ nm, chosen since in the atomistic data any two points of distance $r \leq r_{min}$ are connected. In a second step, points within a sphere of a larger radius $r_{max} = 2.5$ nm are connected with a random acceptance criterion chosen such that the average and minimum coordination numbers observed in the atomistic data are reproduced. This algorithm reproduces the probability of two sites being connected (see the Supporting Information) and retains the same average number of connections per site (coordination number). Transfer integrals J_{ij} for all connected sites have been modeled by mimicking the Gaussian distributions of $\log_{10}(J_{ij}^2/eV^2)$ for sites at a fixed separation, for which the distance-dependent mean and variance values have been calculated from the atomistic data. With point positions, site energies, and electronic couplings at hand we evaluated hopping rates using eq 1. The use of the stochastic model allowed us to study eight times larger systems and, consequently, a wider range of charge densities, down to $\rho = 0.97 \times 10^{17}$ cm^{-3}.

In order to eliminate finite-size effects at small charge densities, an extrapolation procedure has been used, where mobilities are first simulated at elevated temperatures (for the energetic disorder of 0.253 eV an estimate for a nondispersive temperature regime is $T \gtrsim 1700$ K[34]) and then fitted to the relation

$$\mu(T) = \frac{\mu_0}{T^{3/2}} \exp\left(-\left(\frac{a}{T}\right)^2 - \left(\frac{b}{T}\right)\right) \tag{2}$$

which then gives a nondispersive mobility value at room temperature.

In order to fit the mobility-density dependence of the atomistic and stochastic models, Gaussian disorder models where used. They are based on Monte Carlo simulations in lattices that were used for a parametrization of $\mu(\rho, T, F)$ and thus allow the extraction of, e.g., the disorder parameter from experiments. The original version[20] was later extended to include correlated disorder,[21] finite charge density in the extended Gaussian disorder model (EGDM[9]) as well as a combination of both in the extended, correlated Gaussian disorder model (ECDM[22]). Key equations are recapitulated in the Supporting Information.

3. RESULTS

The mobility versus field dependency for the microscopic (atomistic and stochastic) models is shown in Figure 2a. One can see that the mobility increases by 4 orders of magnitude with the increase of charge density from 10^{16} cm^{-3} to 10^{19} cm^{-3}. The reason for this increase is that at high densities deep energetic traps are filled, detrapping the rest of carriers. Since detrapping is stronger than the slow-down due to blocked pathways, the overall mobility increases.[10] One can also see that the stochastic and microscopic simulations agree at high charge densities but are off by orders of magnitude at small densities. The stark disagreement is due to finite-size effects: sampling of the density of states is limited to a relatively small number of site energies (since periodic boundary conditions are used), resulting in logarithmically slow convergence of the carrier energy with system size and hence overestimation of the mobility.[34] Since the microscopic system is eight times smaller

than the stochastic one, the finite size effects are significantly more pronounced (hotter carriers in a smaller simulation box), leading to orders of magnitude differences in mobility values.

For the atomistic and stochastic models, the energetic disorder, σ, zero-field mobility, $\mu_0(300\ K)$, and an effective lattice spacing, a, can be obtained directly from the distribution of site energies, diffusion constant (using the Einstein relation), and material density, respectively. Assuming a cubic lattice, we obtain $a = (V/N)^{1/3} = 0.86$ nm, the variance of site energies $\sigma(1/N\sum_i(E_i - \langle E \rangle)^2)^{1/2} = 0.253$ eV, and $\mu_0(300\ K) = 3.5 \times 10^{-10}$ cm^2/(V s) (for the system of 32000 molecules).

These results can be compared by fits of EGDM and ECDM to the obtained mobility dependence. A direct fit of the data as obtained by the microscopic simulations yields parameters which are completely unphysical, e.g., $\mu_0^{ECDM}(300\ K) \approx 10^{13}$ cm^2/(V s). The reason for this is that the zero-density mobility of the microscopic model is subject to substantial finite-size effects.[34] Extrapolating the microscopic data to a system of an infinite size, as described in the methodology section, we obtain a nondispersive zero-density mobility of $\sim 10^{-17}$ cm^2/(V s), lowering the finite size biased value by seven (!) orders of magnitude. Including this value in the fit then yields physically reasonable parameters.

Fitting results are summarized in Figure 2b and Table 1. Apart from a zero-density point, densities between 7.76×10^{17}

Table 1. Lattice Spacing, Energetic Disorder, and Mobility at Zero Field and Density of the Atomistic, EGDM, and ECDM Models[a]

	a [nm]	σ [eV]	μ_0 (300 K) [cm^2/(V s)]
microscopic	0.86	0.253	2.0×10^{-17}
EGDM	1.79	0.232	2.1×10^{-17}
ECDM	0.34	0.302	3.3×10^{-18}

[a]The value of μ_0 is calculated at 300 K.

cm^{-3} and 6.22×10^{18} cm^{-3} were used, for which the transport is nondispersive at room temperature. One can see that the values for σ and $\mu_0(300\ K)$ obtained from the fit to the EGDM model are very similar to the microscopic model. The value of the lattice constant is, however, significantly larger. The physical reason for this is the absence of spatial correlations in EGDM, which is effectively compensated by an increased hopping range. The ECDM yields a much smaller lattice constant, larger energetic disorder, a smaller value of $\mu_0(300\ K)$. Overall, the ECDM provides a worse fit of the data (smaller slope at high densities), which is surprising since it includes spatial site energy correlations. Both models, of course, incorporate certain assumptions, e.g., they are parametrized on simulations using Miller–Abrahams rates,[56] i.e., without accounting for polaronic effects.[7] The energetic disorder considered in the models ranges from $\sigma = 0.05$ eV up to 0.16 eV (for $T = 300$ K), while an energetic disorder of 0.253 eV is predicted by the microscopic simulations, which is outside the parametrization interval. The main issue, however, lies in spatial correlations. ECDM site energies, E_i, are evaluated as

$$E_i = -\sum_{j \neq i} \frac{q\mathbf{p}_j(\mathbf{r}_j - \mathbf{r}_i)}{\varepsilon |\mathbf{r}_j - \mathbf{r}_i|^3} \qquad (3)$$

where $\mathbf{p}_j$ is a randomly oriented dipole moment of fixed absolute value and ε is the material's relative permittivity. The resulting energetic disorder has a width of $\sigma = 2.35qp/\varepsilon a^2$ [21,57]

and the energy correlation function for a simple cubic lattice can be approximated by[21,22,58] $\kappa(r) = \kappa_0 a\sigma^2 r^{-1}$ with a constant coefficient κ_0. The energetic correlation in this model is fully determined by the energetic disorder, σ, while in microscopic simulations based on realistic morphologies materials with the same energetic disorder may have different strengths of correlation. Furthermore, a comparison of the r^{-1} proportionality in the ECDM to the observed microscopic correlation (see Figure 3) shows that, especially at small distances, the model is
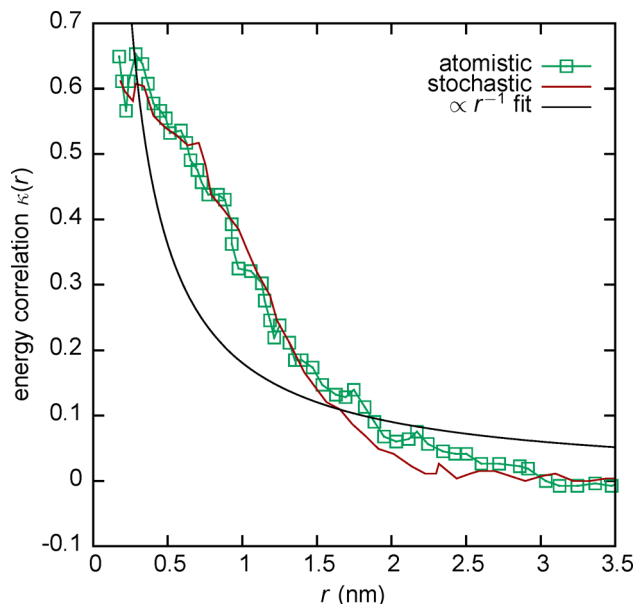
Figure 3. Site energy correlation function, $\kappa(r)$. While the agreement between atomistic and stochastic model is good, the proportionality $\kappa(r) \propto r^{-1}$ assumed in the ECDM fails especially at small distances.

unable to capture the spatial correlation. A possible reason for this is that in DCV4T not only the orientation of dipoles is random, but also their absolute values can differ significantly for different molecules. Indeed, an analysis of the dipole moments in the DCV4T morphology shows that the two most frequent molecular geometry conformations have absolute values of 1.4 and 12.3 D.

Experimental OFET mobility measurements in polycrystalline (or partially amorphous) films report mobilities of 10^{-4} cm^2/(V s)[36,43] (for a carrier density of about 5×10^{18} cm^{-3}). Though the simulated values are reasonable, a direct comparison to experiment is not possible since we study a completely amorphous system: due to increased energetic disorder we obtain two orders of magnitude lower mobility values.

4. CONCLUSIONS

To summarize, we have demonstrated how the dependence of mobility on external field and charge density can be parametrized using atomistic simulations. Two important steps in these procedures are (i) the parametrization of a stochastic network model, which helps to treat large systems and to increase the range of accessible charge densities; (ii) the extrapolation of dispersive mobilities at small charge densities to nondispersive values, thus removing artifacts related to finite size effects inherently present in small periodic systems. For an organic dye considered here, DCV4T, the EGDM provides reasonable fits of the Poole–Frenkel dependencies, compensat-

ing for spatial correlations, which are present in amorphous DCV4T, by a large lattice constant. The ECDM yields worse fitting, in spite of explicit treatment of spatial site energy correlations. This has been shown to be a result of the model correlation differing from the microscopically observed one. The proposed approach relates the chemical structure, morphology, and microscopic transport parameters to an analytical expression for mobility and therefore can be used to optimize organic devices on a macroscopic scale.

■ ASSOCIATED CONTENT

Ⓢ Supporting Information

Parametrization of the stochastic model and of Gaussian disorder models and the extrapolation to nondispersive transport. This material is available free of charge via the Internet at http://pubs.acs.org.

■ AUTHOR INFORMATION

Corresponding Authors
*E-mail: kordt@mpip-mainz.mpg.de (P.K.).
*E-mail: denis.andrienko@mpip-mainz.mpg.de (D.A.).

Notes
The authors declare no competing financial interest.

■ ACKNOWLEDGMENTS

■ REFERENCES

(1) Tang, C. W. *Appl. Phys. Lett.* **1986**, *48*, 183.
(2) Kirchartz, T.; Nelson, J. *Device Modelling of Organic Bulk Heterojunction Solar Cells*; Topics in Current Chemistry; Springer: Berlin Heidelberg, 2013; pp 1−46.
(3) Blom, P.; De Jong, M. *IEEE J. Sel. Top. Quantum Electron.* **1998**, *4*, 105−112.
(4) Tsumura, A.; Koezuka, H.; Ando, T. *Appl. Phys. Lett.* **1986**, *49*, 1210.
(5) Baranovskii, S. D.; Rubel, O.; Thomas, P. *J. Non-Cryst. Solids* **2006**, *352*, 1644−1647.
(6) Brondijk, J. J.; Maddalena, F.; Asadi, K.; van Leijen, H. J.; Heeney, M.; Blom, P.W. M.; de Leeuw, D. M. *Phys. Status Sol. (b)* **2012**, *249*, 138−141.
(7) Fishchuk, I. I.; Arkhipov, V. I.; Kadashchuk, A.; Heremans, P.; Bassler, H. *Phys. Rev.B* **2007**, *76*, 045210.
(8) Meyertholen, A. D.; Li, Z. Q.; Basov, D. N.; Fogler, M. M.; Martin, M. C.; Wang, G. M.; Dhoot, A. S.; Moses, D.; Heeger, A. J. *Appl. Phys. Lett.* **2007**, *90*, 222108.
(9) Pasveer, W. F.; Cottaar, J.; Tanase, C.; Coehoorn, R.; Bobbert, P. A.; Blom, P. W. M.; de Leeuw, D. M.; Michels, M. A. J. *Phys. Rev. Lett.* **2005**, *94*, 206601.
(10) Tanase, C.; Blom, P. W. M.; de Leeuw, D. M.; Meijer, E. J. *Phys. Status Sol. (a)* **2004**, *201*, 1236−1245.
(11) Kreouzis, T.; Poplavskyy, D.; Tuladhar, S. M.; Campoy-Quiles, M.; Nelson, J.; Campbell, A. J.; Bradley, D. D. C. *Phys. Rev. B* **2006**, *73*, 235201.
(12) Tuladhar, S. M.; Poplavskyy, D.; Choulis, S. A.; Durrant, J. R.; Bradley, D. D. C.; Nelson, J. *Adv. Funct. Mater.* **2005**, *15*, 1171−1182.
(13) Anthopoulos, T. D.; Singh, B.; Marjanovic, N.; Sariciftci, N. S.; Ramil, A. M.; Sitter, H.; Cölle, M.; Leeuw, D. M. d. *Appl. Phys. Lett.* **2006**, *89*, 213504.
(14) Lee, J. Y.; Roth, S.; Park, Y. W. *Appl. Phys. Lett.* **2006**, *88*, 252106.
(15) Zaumseil, J.; Sirringhaus, H. *Chem. Rev.* **2007**, *107*, 1296−1323.
(16) Marcon, V.; Breiby, D. W.; Pisula, W.; Dahl, J.; Kirkpatrick, J.; Patwardhan, S.; Grozema, F.; Andrienko, D. *J. Am. Chem. Soc.* **2009**, *131*, 11426−11432.
(17) Juška, G.; Arlauskas, K.; Viliūnas, M. M.; Kočka, J. *Phys. Rev. Lett.* **2000**, *84*, 4946−4949.
(18) Tanase, C.; Meijer, E. J.; Blom, P. W. M.; de Leeuw, D. M. *Phys. Rev. Lett.* **2003**, *91*, 216601.
(19) Borsenberger, P.; Pautmeier, L.; Bassler, H. *J. Chem. Phys.* **1991**, *94*, 5447.
(20) Bässler, H. *Phys. Status Sol. (b)* **1993**, *175*, 15−56.
(21) Novikov, S.; Dunlap, D.; Kenkre, V.; Parris, P.; Vannikov, A. *Phys. Rev. Lett.* **1998**, *81*, 4472−4475.
(22) Bouhassoune, M.; Mensfoort, S. v.; Bobbert, P.; Coehoorn, R. *Org. Electron.* **2009**, *10*, 437−445.
(23) Mauer, R.; Kastler, M.; Laquai, F. *Adv. Funct. Mater.* **2010**, *20*, 2085−2092.
(24) Kastler, M.; Laquai, F.; Müllen, K.; Wegner, G. *Appl. Phys. Lett.* **2006**, *89*, 252103.
(25) Laquai, F.; Hertel, D. *Appl. Phys. Lett.* **2007**, *90*, 142109.
(26) Katsouras, I.; Najafi, A.; Asadi, K.; Kronemeijer, A. J.; Oostra, A. J.; Koster, L. J. A.; de Leeuw, D. M.; Blom, P. W. M. *Org. Electron.* **2013**, *14*, 1591−1596.
(27) Mihailetchi, V. D.; Xie, H. X.; de Boer, B.; Koster, L. J. A; Blom, P. W. M. *Adv. Funct. Mater.* **2006**, *16*, 699−708.
(28) Ruhle, V.; Lukyanov, A.; May, F.; Schrader, M.; Vehoff, T.; Kirkpatrick, J.; Baumeier, B.; Andrienko, D. *J. Chem. Theory Comput.* **2011**, *7*, 3335−3345.
(29) Athanasopoulos, S.; Kirkpatrick, J.; Martinez, D.; Frost, J. M.; Foden, C. M.; Walker, A. B.; Nelson, J. *Nano Lett.* **2007**, *7*, 1785−1788.
(30) Nelson, J.; Kwiatkowski, J. J.; Kirkpatrick, J.; Frost, J. M. *Acc. Chem. Res.* **2009**, *42*, 1768−1778.
(31) Palermo, M. F.; Pizzirusso, A.; Muccioli, L.; Zannoni, C. *J. Chem. Phys.* **2013**, *138*, 204901.
(32) Baumeier, B.; Stenzel, O.; Poelking, C.; Andrienko, D.; Schmidt, V. *Phys. Rev. B* **2012**, *86*, 184202.
(33) Stenzel, O.; Hirsch, C.; Brereton, T.; Baumeier, B.; Andrienko, D.; Kroese, D. P.; Schmidt, V. *Multiscale Model. Simul.* **2014**.
(34) Lukyanov, A.; Andrienko, D. *Phys. Rev. B* **2010**, *82*, 193202.
(35) Koerner, C.; Elschner, C.; Miller, N. C.; Fitzner, R.; Selzer, F.; Reinold, E.; Bäuerle, P.; Toney, M. F.; McGehee, M. D.; Leo, K.; Riede, M. *Org. Electron.* **2012**, *13*, 623−631.
(36) Fitzner, R.; Elschner, C.; Weil, M.; Uhrich, C.; Körner, C.; Riede, M.; Leo, K.; Pfeif-fer, M.; Reinold, E.; Mena-Osteritz, E.; Bauerle, P. *Adv. Mater.* **2012**, *24*, 675−680.
(37) Cheng, Y.-J.; Yang, S.-H.; Hsu, C.-S. *Chem. Rev.* **2009**, *109*, 5868−5923.
(38) Fitzner, R.; Reinold, E.; Mishra, A.; Mena-Osteritz, E.; Ziehlke, H.; Korner, C.; Leo, K.; Riede, M.; Weil, M.; Tsaryova, O.; Weiβ, A.; Uhrich, C.; Pfeiffer, M.; Bauerle, P. *Adv. Funct. Mater.* **2011**, *21*, 897−910.
(39) Mishra, A.; Ma, C.-Q.; Bäuerle, P. *Chem. Rev.* **2009**, *109*, 1141−1276.
(40) Schulze, K.; Uhrich, C.; Schüppel, R.; Leo, K.; Pfeiffer, M.; Brier, E.; Reinold, E.; Bauerle, P. *Adv. Mater.* **2006**, *18*, 2872−2875.
(41) Baumeier, B.; Andrienko, D.; Ma, Y.; Rohlfing, M. *J. Chem. Theory Comput.* **2012**, *8*, 997−1002.
(42) Baumeier, B.; Andrienko, D.; Rohlfing, M. *J. Chem. Theory Comput.* **2012**, *8*, 2790−2795.
(43) Schrader, M.; Fitzner, R.; Hein, M.; Elschner, C.; Baumeier, B.; Leo, K.; Riede, M.; Bauerle, P.; Andrienko, D. *J. Am. Chem. Soc.* **2012**, *134*, 6052−6056.

(44) Elschner, C.; Schrader, M.; Fitzner, R.; Levin, A. A.; Bauerle, P.; Andrienko, D.; Leo, K.; Riede, M. *RSC Adv.* **2013**, *3*, 12117−12123.

(45) Schrader, M.; Körner, C.; Elschner, C.; Andrienko, D. *J. Mater. Chem.* **2012**, *22*, 22258.

(46) Jorgensen, W. L.; Tirado-Rives, J. *J. Am. Chem. Soc.* **1988**, *110*, 1657−1666.

(47) Jorgensen, W. L.; Maxwell, D. S.; Tirado-Rives, J. *J. Am. Chem. Soc.* **1996**, *118*, 11225−11236.

(48) Hess, B.; Kutzner, C.; van der Spoel, D.; Lindahl, E. *J. Chem. Theory. Comput.* **2008**, *4*, 435−447.

(49) Berendsen, H. J. C.; Postma, J. P. M.; Gunsteren, W. F. v.; DiNola, A.; Haak, J. R. *J. Chem. Phys.* **1984**, *81*, 3684−3690.

(50) Marcus, R. A. *Rev. Mod. Phys.* **1993**, *65*, 599−610.

(51) Hutchison, G. R.; Ratner, M. A.; Marks, T. J. *J. Am. Chem. Soc.* **2005**, *127*, 2339−2350.

(52) Thole, B. T. *Chem. Phys.* **1981**, *59*, 341−350.

(53) van Duijnen, P. T.; Swart, M. *J. Phys. Chem. A* **1998**, *102*, 2399−2407.

(54) Ridley, J.; Zerner, M. *Theor. Chim. Acta* **1973**, *32*, 111−134.

(55) Kirkpatrick, J. *Int. J. Quantum Chem.* **2008**, *108*, 51−56.

(56) Miller, A.; Abrahams, E. *Phys. Rev.* **1960**, *120*, 745−755.

(57) Young, R. H. *Philos. Mag. Part B* **1995**, *72*, 435−457.

(58) Novikov, S. V.; Vannikov, A. V. *J. Phys. Chem.* **1995**, *99*, 14573−14576.